Kinetics and Thermochemistry of the OH Radical Reaction with CF_3CCl_2H and CF_3CFClH

Takahiro Yamada,[†] Tunchen D. Fang,[‡] Philip H. Taylor,*[,†] and Rajiv J. Berry[§]

Environmental Sciences and Engineering Group, University of Dayton Research Institute, 300 College Park, Dayton, Ohio 45469-0132, Physical Optics Corporation, 2545 W. 237th Street, Suite B, Torrance, California, 90505-5228, and Center for Computational Modeling of Nonstructural Materials, WL/MLBT, Wright-Patterson AFB, Ohio 45433

Received: October 6, 1999; In Final Form: March 15, 2000

Rate coefficients are reported for the gas-phase reaction of hydroxyl (OH) radicals with CF_3CCl_2H (k_1) and CF_3CFClH (k_2) over an extended temperature range. The measurements were performed using a laser photolysis/laser-induced fluorescence (LP/LIF) technique under slow flow conditions at a total pressure of 740 ± 10 Torr. The lower temperature measurements for k_1 and k_2 were in agreement with previous measurements using different techniques. Arrhenius plots of the data exhibit significant curvature and were best described by the following modified Arrhenius expressions (cm^3 molecule^{-1} s^{-1}, 2σ error limits): k_1 (296−866 K) = (2.20 ± 0.25) × 10^{-19} $T^{2.26\pm0.10}$ exp(−226 ± 51)/T and k_2 (297−867 K) = (7.72 ± 0.60) × 10^{-20} $T^{2.35\pm0.06}$ exp(−458 ± 30)/T. The experimental measurements were analyzed within the context of transition state theory to provide accurate modified Arrhenius expressions that are applicable to flame conditions. Ab initio calculations were used to evaluate the thermochemical properties of the reactants and products and the partition functions of reactants and their activated complexes. Hydrogen bond dissociation energies (BDE) were also estimated based on calculated enthalpies of formation of reactants and products. An asymmetrical Eckart potential was performed to account for tunneling correction. The resulting TST-based modified Arrhenius expressions (cm^3 molecule^{-1} s^{-1}) were k_1 (250−2000 K) = 3.25 × 10^{-21} $T^{2.88}$ exp(−52/T) and k_2 (250−2000 K) = 4.52 × 10^{-22} $T^{3.18}$ exp(−362/T). The TST-based modified Arrhenius expression is compared to previous TST and SAR predictions. The results of this study indicate that F substitution at the reaction site has a significant (reductive) effect on hydrochlorofluorocarbon (HCFC) reactivity. This result was also observed in our prior studies of $CHFCl_2$ and CHF_2Cl.[4] A similar effect in HCFC reactivity was not observed for changes in F substitution β to the reaction site,[6] indicating that the electron-withdrawing effects of the F atoms are limited to the vicinity of the reaction site.

Introduction

The fate of anthropogenic halogenated hydrocarbons that are released to the atmosphere in the course of various industrial or technological activities is of great environmental concern. In addition to their well-known connection to stratospheric ozone destruction, these compounds are effective greenhouse gases.

Among the most important processes contributing to the destruction of halogenated hydrocarbons, both under atmospheric conditions[1] and at high-temperature incineration/combustion conditions,[2,3] is reaction with hydroxyl (OH) free radicals. To accurately model halogenated hydrocarbon combustion, accurate semiempirical Arrhenius parameters describing rate behavior over extended temperature ranges are required. This paper is the last of a series of our studies for C_1 and C_2 hydrochlorofluorocarbons (HCFCs). With the exception of our recent studies of $CHFCl_2$,[4] CHF_2Cl,[4] CH_3CF_2Cl,[5] CH_2ClCF_2Cl,[6] and CH_2ClCF_3,[6] previous measurements have only been reported over a narrow low-temperature range encompassing tropospheric and stratospheric conditions.[1] At temperatures above 480 K, the prediction of rate constants for these compounds has been previously based solely on conventional transition-state theory (TST)[7,8] and structure−activity relationship (SAR) calculations.[9] Rate coefficient measurements over an extended temperature range are needed to verify and/or refine previously published TST and SAR models.

In this manuscript, we report high-precision rate coefficients for the reaction of OH with CF_3CCl_2H (k_1) and CF_3CFClH (k_2) over an extended temperature range:

$$CF_3CCl_2H + OH \rightarrow CF_3CCl_2 + H_2O \qquad k_1 \qquad \Delta H_{rxn}^{\circ}{}_{298} = -22.47 \text{ kcal/mol}^{10} \quad (1)$$

$$CF_3CFClH + OH \rightarrow CF_3CFCl + H_2O \qquad k_2 \qquad \Delta H_{rxn}^{\circ}{}_{298} = -18.50 \text{ kcal/mol}^{10} \quad (2)$$

Arrhenius plots of the data exhibit significant curvature and were analyzed within the context of bimolecular transition-state theory. Ab initio calculations and isodesmic reactions were used to evaluate the thermochemical properties of the reactants and the partition functions of reactants and their activated complexes. An asymmetric Eckart potential was used to account for tunneling correction. The TST-based modified Arrhenius expression is compared to previous TST and SAR predictions.

* To whom correspondence should be addressed.
[†] University of Dayton Research Institute. Tel.: (937)229-3604. Fax: (937)229-2503. E-mail: taylorph@udri.udayton.edu.
[‡] Physical Optics Corporation. Tel.: (310)530-1416. Fax: (310)530-4577. E-mail: (310)530-4577.
[§] Center for Computational Modeling of Nonstructural Materials. Tel.: (937)225-2467. Fax: (937)255-9019. E-mail: Berryrj@ml.wpafb.af.mil.

10.1021/jp993577f CCC: $19.00
Published on Web 05/05/2000

Experimental Approach and Data Reduction

The experimental procedures were similar to our previous studies of OH reactions with C_1 and C_2 HCFCs.[4−6,11] As a result, we only briefly summarize the procedures here.

OH radicals were produced by 193-nm photodissociation of HCFC/N_2O/H_2O/He gas mixtures with an ArF excimer laser (Questek model 2840). Initial concentrations of the OH precursors, N_2O and H_2O, were $8.7-110.0 \times 10^{12}$ molecules cm^{-3} and $3.2-14.4 \times 10^{15}$ molecules cm^{-3}, respectively. Initial OH concentrations, $[OH]_0$, ranged from 6×10^9 to 2×10^{10} molecules cm^{-3} and were determined from the measured excimer laser fluence and published values of the N_2O absorption coefficient (8.95×10^{-20} cm^2 $molecule^{-1}$ at 298 K),[12] a photodissociation quantum yield for $O(^1D)$ production of unity,[13] and the rapid reaction of $O(^1D)$ with H_2O yielding 2 OH (95% conversion in <20 μs). Experiments were typically conducted for photolysis energy fluences of 1 mJ cm^{-2}. Following reaction initiation, time-resolved OH profiles were measured as functions of HCFC concentration using laser-induced fluorescence with a pulsed Nd:YAG pumped-dye laser (Quanta Ray model DCR-1/PDL-2) emitting at the wavelength of 282.15 nm. The typical energy fluence was 200 μJ/pulse. Broadband fluorescence was collected at 309 nm using a PMT/band-pass filter combination.

Four symmetrical ceramic heaters were used to provide isothermal conditions within the detection volume (reaction zone) of the optical reactor. The gas temperature was measured with a chromel−alumel thermocouple positioned ~2 mm from the probe intersection volume. Measurements using a second retractable chromel−alumel thermocouple indicated a variation of less than 3.5 K across the detection volume for gas temperatures ranging from 295 to 1000 K.

All experiments were carried out under slow flow conditions, and the buildup of reaction products was minimized. Individually controlled gas flows of HCFC/N_2O/ H_2O/He were thoroughly mixed before entering the optical reactor. The composite flow conditioned the reactor for five minutes prior to the onset of data collection, thereby minimizing any effects due to reactant adsorption on the reactor walls. Flow rates were controlled with differential flow transducers, and the total volumetric flow rate just downstream of the reactor was measured before and after each experiment with a bubble meter. All experiments were conducted at a total pressure of 740 ± 10 Torr. Stock samples of CF_3CCl_2H and CF_3CFClH were obtained from PCR, Inc. Typically, 5 to 10 volume % of each stock sample was prepared in previously cleaned and dried 1 L (nominal) Pyrex bulbs at 740 ± 10 Torr and introduced into the gas mixture and delivery system using a calibrated syringe pump (Sage Instruments, 341B). Initial concentrations varied from 4×10^{14} to 4.5×10^{15} molecule cm^{-3} for CF_3CCl_2H and from 1×10^{15} to 1.2×10^{16} molecule cm^{-3} for CF_3CFClH.

Over the entire temperature range, reactive and diffusive OH radical decay profiles exhibited exponential behavior and were fit by the following nonlinear expression:

$$[OH] = [OH]_0 \exp(-k't) + \gamma \qquad (3)$$

where γ is the constant background signal level and t is the time delay between the two lasers. Because $[HCFC]_0 > 1000\text{-}[OH]_0$ in all reactive experiments, exponential OH radical decays of the pseudo-first-order decay constant $k' = k[HCFC] + k_d$ were observed. k_d is the first-order rate constant for OH radical disappearance from the probe volume due to diffusion and reaction with impurities in the carrier gas. The bimolecular rate constant, k, was obtained from the slope of the least-squares straight line through the plot of k′ versus [HCFC], as illustrated for CF_3CCl_2H in Figure 1.

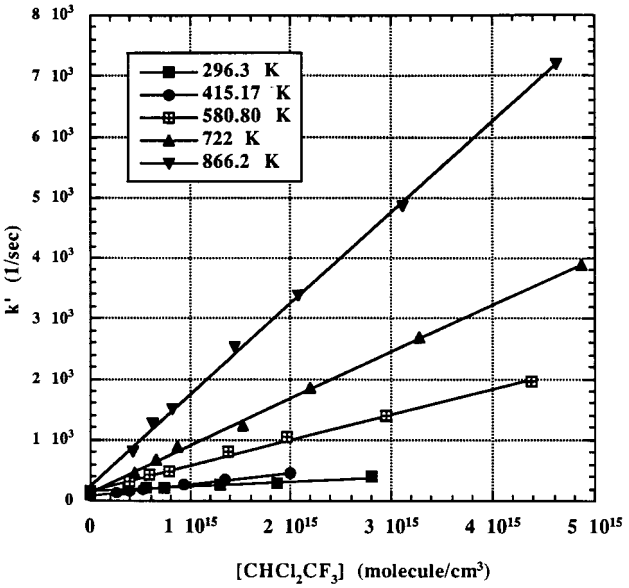

Figure 1. Plot of pseudo-first-order rate coefficient, k', versus [CF_3CCl_2H] for five reaction temperatures.

TABLE 1: Absolute Rate Coefficients for k_1[a]

temperature, K	10^{14} k_1 (cm^3 $molecule^{-1}$ sec^{-1})	temperature, K	10^{14} k_1 (cm^3 $molecule^{-1}$ sec^{-1})
296.3	3.67 ± 0.24	460.2	14.77 ± 0.21
308.6	4.14 ± 0.22	479.6	15.29 ± 0.36
318.6	4.78 ± 0.11	510.6	19.83 ± 0.42
334.7	5.93 ± 0.21	545.1	22.61 ± 0.86
347.5	6.13 ± 0.45	580.8	25.17 ± 0.93
363.2	6.86 ± 0.18	619.5	29.21 ± 0.42
377.5	7.92 ± 0.32	666.5	36.50 ± 1.09
397.3	9.92 ± 0.16	722.0	45.45 ± 1.11
415.2	10.63 ± 0.21	786.3	55.52 ± 1.90
438.6	13.32 ± 0.46	866.2	86.38 ± 2.01

[a] Errors represent $\pm 2\sigma$.

TABLE 2: Absolute Rate Coefficients for k_2[a]

temperature, K	10^{14} k_2 (cm^3 $molecule^{-1}$ sec^{-1})	temperature, K	10^{14} k_2 (cm^3 $molecule^{-1}$ sec^{-1})
296.8	1.08 ± 0.16	460.2	4.98 ± 0.20
308.0	1.19 ± 0.11	481.2	5.43 ± 0.24
319.7	1.33 ± 0.05	511.1	7.64 ± 0.27
334.4	1.81 ± 0.10	544.5	8.74 ± 0.49
347.0	2.05 ± 0.05	580.0	10.57 ± 0.57
362.4	2.45 ± 0.11	620.5	14.18 ± 0.40
377.5	2.85 ± 0.11	666.7	17.00 ± 0.69
396.7	3.48 ± 0.16	721.4	21.45 ± 0.61
415.2	3.76 ± 0.17	786.1	27.79 ± 1.14
438.0	4.33 ± 0.16	866.7	39.59 ± 1.29

[a] Errors represent $\pm 2\sigma$.

Gas chromatography−mass spectrometry (GC-MS) analyses indicated that both HCFC substrates were free of contaminants (>99.9% pure). The remaining chemicals used in our gas delivery system had the following stated minimum purities: He (99.999+%); N_2O (99.9%); and H_2O (HPLC organic-free reagent grade).

Experimental Results

Absolute rate constants for k_1 and k_2 are presented in Tables 1 and 2, respectively. Random error limits ($\pm 2\sigma$) derived from a propagation of error analysis ranged from 3% to 9% with a

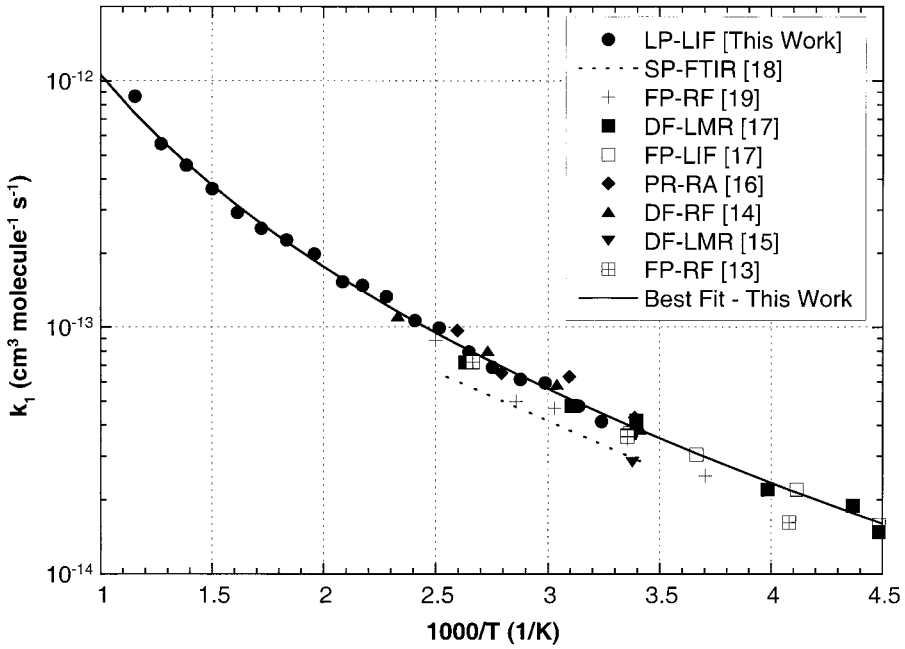

Figure 2. Arrhenius plot of experimental measurements for k_1. Also shown are prior experimental studies (delineated by the experimental method) at lower temperatures and the empirical "best fit" curve through the data.[14−20]

vast majority of the values <5%. The possibility that OH decays could be due to reaction with photolytically generated but unreacted $O(^1D)$ atoms was investigated by varying the H_2O concentration. Bimolecular rate determinations were unaffected by 5-fold changes in $[H_2O]$, indicating that unreacted $O(^1D)$ atoms had no effect on the observed measurements. The production of NO from the reaction of $O(^1D)$ with N_2O was also considered as a possible source of secondary reactions.[12] Using numerical simulations, NO concentrations were found to be insignificant under our experimental conditions (<2% of the initial $[OH]_0$). The production of ClO radicals from the reaction of $O(^1D)$ with the substrate could not be evaluated numerically due to the lack of knowledge of the branching ratio for ClO production.[12] The measured OH decay rates indicate that combination of OH with ClO radicals was negligible under our experimental conditions.

In the absence of reactant impurities and secondary reactions, sources of systematic error were then limited to thermally and photolytically induced secondary reactions. The possibility of thermal artifacts was investigated by varying the total gas flow rate. k_1 and k_2 were found to be independent of residence time in the high-temperature region, implying a lack of thermal reaction of the substrates at the highest temperatures of these studies. The effect of laser photolysis on the substrate was observed to be insignificant based on numerous experiments, in which a 4-fold variation of the excimer laser intensity (0.5−2 mJ cm^{-2}) had no observable effect on OH decays.

As illustrated in Figures 2 and 3, to our knowledge this is the first report of experimental measurements for these reactions above temperatures of 480 K. Also shown in Figures 2 and 3 are previous measurements at lower temperatures reported using different techniques.[14−20] Examination of the rate measurements for k_1 indicates that our room temperature rate measurements were in excellent agreement with those previously reported by Watson et al. (3.67×10^{-14} cm^3 molecule^{-1} s^{-1} vs 3.60×10^{-14} cm^3 molecule^{-1} s^{-1}).[14] Although the recent relative rate measurement of Hsu and DeMore[19] is systematically 20−30% lower than the direct rate measurements, the deviation between our measurements and all previous measurements[14−20] obtained between 296 and 429 K is within combined error limits. For k_2, our room-temperature rate measurements were 15% smaller than that reported by Howard and Evenson (1.08×10^{-14} cm^3 molecule^{-1} s^{-1} vs 1.24×10^{-14} cm^3 molecule^{-1} s^{-1})[16] and ∼15−25% larger than the other previously reported rate measurements.[14,18,19] Overall, comparison of our measurements with the other previous measurements obtained between 297 and 425 K are within combined error limits.

The Arrhenius plots for k_1 and k_2 demonstrated significant curvature, particularly above 500 K. A nonlinear least-squares fit of our data (weighted at $\omega_k = 1/\sigma_k^2$) to the modified Arrhenius equation $k = AT^n \exp(-B/T)$ produced the following expressions, denoted as "best fit" in Figures 2 and 3:

$$k_1(296-866\ \text{K}) = (2.20 \pm 0.25) \times 10^{-19}\, T^{2.26\pm0.10} \exp(-226 \pm 51)/T \quad (2)$$

$$k_2(297-867\ \text{K}) = (7.72 \pm 0.60) \times 10^{-20}\, T^{2.35\pm0.06} \exp(-458 \pm 30)/T \quad (3)$$

The error limits ($\pm 2\sigma$) were derived from an iterative χ^2 minimization technique (least squares). The large temperature exponents in eqs 2 and 3 are indicative of the substantial degree of curvature in the Arrhenius plot. This best fit expression for k_1, when extrapolated to lower temperatures, is in good agreement with the recent measurements of Gierczak et al.[18] A similar extrapolation of the best fit expression for k_2 results in a 20−50% overestimation of the rate constant compared with the recent measurements of Gierczak et al.[18] and the older measurements of Watson et al.[14]

Theoretical Methods

Arrhenius plots of k_1 and k_2 exhibit significant curvature and were analyzed within the context of bimolecular transition-state theory. Ab initio calculations were performed using Gaussian code[21,22] on Cray Y-MP, C-90, HP−PARisk, SGI Power-Challenge, and SGI Origin 2000 computers. A composite ab initio method G2(MP2)[23] was used to calculate the energies of

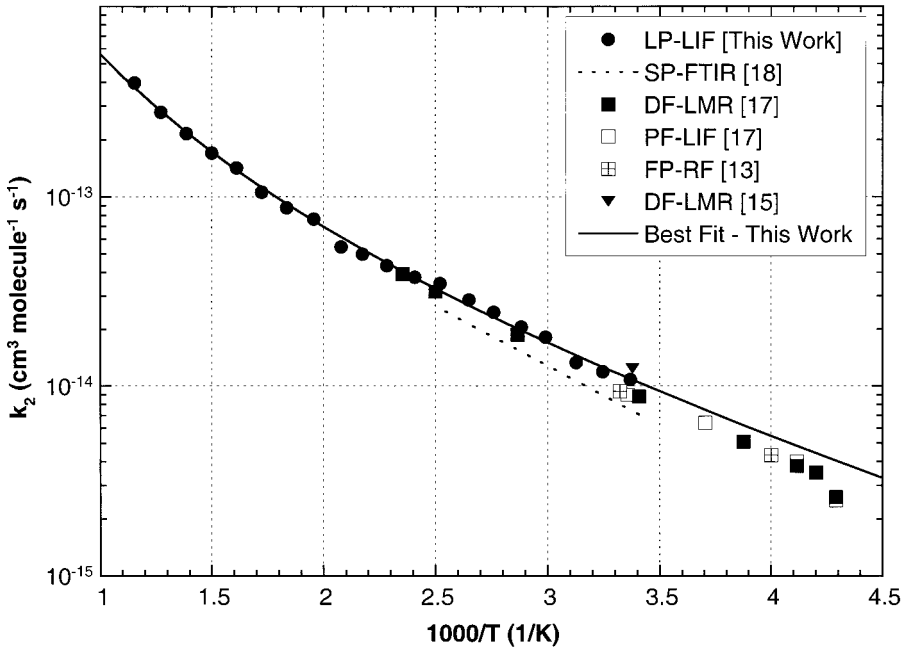

Figure 3. Arrhenius plot of experimental measurements for k_2. Also shown are prior experimental studies (delineated by the experimental method) at lower temperatures and the empirical "best fit" curve through the data.[14,16,18,19]

reactants, transition states (TSs), and products. G2(MP2) was also performed for several fluorinated and chlorinated ethanes, ethane, and the ethyl radical, which were used for isodesmic reactions. Frequencies and zero-point energy (zpe) were calculated at the HF/6-31G(d) level of theory, and geometries were optimized at the MP2(full)/6-31G(d) level of theory.

Enthalpies of Formation. Enthalpies of formation ($\Delta H_f^\circ{}_{298}$) for CF_3CCl_2H, CF_3CFClH, $CF_3C{\cdot}Cl_2$ and $CF_3C{\cdot}FCl$ were estimated using the total energies obtained by the G2(MP2) composite ab initio calculation method[23] and isodesmic reactions. Hydrogen bond dissociation energies (BDEs) for CF_3CCl_2H and CF_3CFClH were also calculated. Zero-point energy and thermal correction to 298.15 K[24] were calculated with frequencies scaled by 0.8929, as widely used in theoretical thermochemical calculations for frequencies determined at the HF/6-31G(d) level of theory.[24] The isodesmic reactions employed were

For CF_3CCl_2H:

$$CF_3CCl_2H + C_2H_6 = CF_3CH_3 + CCl_2HCH_3 \quad (4)$$

For CF_3CFClH:

$$CF_3CFClH + C_2H_6 = CF_3CH_3 + CFClHCH_3 \quad (5)$$

For $CF_3C{\cdot}Cl_2$: $CF_3C{\cdot}Cl_2 + C_2H_6 = CF_3CCl_2H + C_2H_5$ (6)

For $CF_3C{\cdot}FCl$:

$$CF_3C{\cdot}FCl + C_2H_6 = CF_3CFClH + C_2H_5 \quad (7)$$

The isodesmic reaction method relies upon the similarity of bond type in the reactants and products, leading to a cancellation of systematic errors in the ab initio calculations.[24] An isodesmic reaction requires bond-type conservation: the number of each formal chemical bond type is conserved in the reaction. Applying the isodesmic reaction method will lead to more accurate results if groups are conserved; group conservation allows correlation of next-nearest-neighbor atoms in reactants and products in addition to bond types.[25] Reactions 4 and 5 conserve both bond types and groups, and reactions 6 and 7 conserve bond types.

G2(MP2) composite calculations were performed for all species in reaction 1, and the enthalpy of reaction ($\Delta H_{rxn}^\circ{}_{298}$) was calculated. The evaluated literature data for $\Delta H_f^\circ{}_{298}$ were substituted for C_2H_6[26] (−20.04 kcal/mol), CF_3CH_3[27] (−178.94 kcal/mol), and CCl_2HCH_3[28] (−30.50 kcal/mol); then, the $\Delta H_f^\circ{}_{298}$ of CF_3CCl_2H was calculated. $\Delta H_f^\circ{}_{298}$ of CF_3CFClH, $CF_3C{\cdot}Cl_2$ and $CF_3C{\cdot}FCl$ were calculated in the same manner. Hydrogen BDEs were evaluated based on the calculated $\Delta H_f^\circ{}_{298}$ of reactants and products using a literature value of hydrogen atom[29] (52.1 kcal/mol).

Standard Entropy and Heat Capacities and Hindered Rotational Contribution to Thermodynamic Parameters. Harmonic vibrational frequencies calculated at the HF/6-31G(d) level of theory and the moments of inertia from molecular structures optimized at MP2(full)/6-31G(d) were used to calculate the entropy (S°_{298}) and heat capacity ($C_p(T)$) (except the C−C torsional mode) for reactants and products. Contribution to S°_{298} and $C_p(T)$s from the C−C torsional mode was estimated using the technique for the calculation of thermodynamic functions from hindered rotations with arbitrary potentials.[25,30,31] The technique employs expansion of the hindrance potential in a Fourier series, calculation of the Hamiltonian matrix in the basis of the wave functions of free internal rotation, and subsequent calculation of energy levels by direct diagonalization of the Hamiltonian matrix. The torsional potential calculated at discrete torsional angles is represented by a truncated Fourier series. All potential curves of rotational barrier versus dihedral angle were fit by a truncated Fourier series:

$$V(\text{Ø}) = a_0 + a_1\cos(\text{Ø}) + a_2\cos(2\text{Ø}) + a_3\cos(3\text{Ø}) + b_1\sin(\text{Ø}) + b_2\sin(2\text{Ø}) + b_3\sin(3\text{Ø}) \quad (8)$$

where values of the coefficients a_i were calculated to provide the minimum and maxima of the torsional potentials.

The Hamiltonian matrix was then truncated to the size of $2K_{max} + 1$, where K_{max} is the maximum rotational quantum

TABLE 3: Calculated Frequencies[a] (HF/6-31G(d)) and Rotational Constants[b] (MP2(full)/6-31G(d))

	CF_3CCl_2H	CF_3CFClH	CF_3CCl_2-H-OH	$CF_3CFCl-H-OH$	$CF_3C\cdot Cl_2$	$CF_3C\cdot FCl$
1	71*[c]	72*	3120i[d]	3053i[d]	41*	53*
2	181	180	61*	54*	157	173
3	206	228	74	60	181	202
4	256	312	90	87	242	308
5	347	369	113**[e]	114**	354	378
6	368	436	182	177	386	444
7	509	512	200	222	463	510
8	543	558	245	306	547	562
9	656	679	326	326	575	641
10	749	803	351	379	699	738
11	836	876	390	450	937	961
12	863	1123	520	523	959	1199
13	1169	1188	544	560	1222	1230
14	1233	1253	667	694	1264	1269
15	1259	1314	735	773	1304	1360
16	1297	1318	806	847		
17	1354	1405	873	911		
18	3009	3003	916	1032		
19			1024	1167		
20			1249	1255		
21			1269	1274		
22			1289	1336		
23			1434	1474		
24			3596	3598		
I_a	2.089	3.157	1.362	1.725	2.112	3.208
I_b	1.698	1.790	1.187	1.475	1.668	1.766
I_c	1.137	1.455	1.126	1.186	1.117	1.429

[a] Unit in cm^{-1}. Scaled by 0.8929. [b] Unit in GHz. [c] * corresponds to C−C torsional frequency. [d] Imaginary frequency. [e] ** corresponds to −OH torsional frequency.

number considered. The truncated matrix (in reduced dimensionless form) was diagonalized, and the eigenvalues were used to calculate the partition function, entropy, heat capacity, and so forth. This was accomplished using direct summation over the calculated energy levels according to standard expressions of statistical thermodynamics.[32] Two of Yamada et al.'s previous reports studying thermodynamic properties of hydrofluoroethanes[31] and hydrofluoropropanes[33] using this method show good agreement with existing literature data. The maximum deviation from literature data[34] for the hydrofluoroethanes, which have three fluorines on one carbon site, were 0.64 cal/(mol K) for $S°_{298}$ and 0.24 cal/(mol K) for $C_p(T)$s ($300 \leq T/K \leq 1500$).

Rate Constant Calculation. Rate constants were estimated using the Eyring TST expression:[35]

$$k_{TST} = \Gamma(k_b T/h)(Q_{TS}/Q_{Rct})\exp(-\Delta E^{\ddagger}_e/RT) \qquad (9)$$

where: Γ is the tunneling factor; Q_{TS} and Q_{Rct} are the partition functions of the transition state and reactants; and $\Delta E^{\ddagger}_e$ is the difference in energy between the initial substances and the activated state at absolute zero.

The partition functions were calculated using MP2(full)/6-31G(d)-determined moments of inertia and HF/6-31G(d)-determined frequencies (scaled by 0.8929), along with statistical mechanics.[36] The method presented by Schwartz et al.[37] for hydrogen abstraction from fluoromethanes by the hydroxyl radical was employed in this study. A detailed description can be found in their paper.[37] The experimental splitting of 139.7 cm^{-1} in the $^2\Pi$ ground state was used to calculate the electronic partition function of the OH radical.[38] Vibrations were treated as harmonic oscillators except for C−C torsional modes of reactants and C−C and −OH torsional modes of the transition states, which were treated as hindered internal rotors using the polynomial expression proposed by Ayala and Schlegel to calculate the partition function for the hindered rotor (Q_{HR}).[39] The CF_3C and OH group moments were treated as linear along the C−H−O axis. This yields reduced moments of inertia $I_r = 1.54 \times 10^{-47}$ kg m^2 for the reactions of the two compounds.

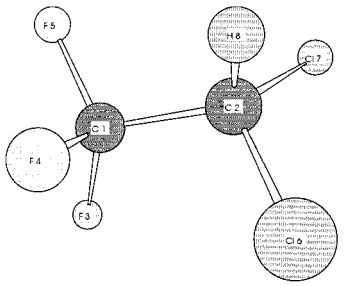

Bond Length	Å	Bond Angle	Degree
C1-C2	1.525	∠C2C1F3	112.2
C1-F3	1.337	∠C2C1F4	109.7
C1-F4	1.344	∠C2C1F5	109.7
C1-F5	1.344	∠C1C2Cl6	109.9
C2-Cl6	1.761	∠C1C2Cl7	109.9
C2-Cl7	1.761	∠C1C2H8	107.7
C2-H8	1.089		

Figure 4. MP2(full)/6-31G(d) optimized geometry (CF_3CCl_2H).

The tunneling factor, Γ, was calculated using an asymmetrical Eckart potential function.[40] The imaginary frequencies obtained at the HF/6-31G(d) level of theory and barriers determined from G2(MP2) energies of reactants and TSs were adjusted to fit experimental results, instead of evaluating the tunneling using the internal reaction coordinate (IRC). The tunneling factors were calculated using Erwin-Henry computer code.[41]

Theoretical Results

Frequency and Geometry. Table 3 shows frequencies and moments of inertia of reactants, TSs, and products calculated at HF/6-31G(d) and MP2(full)/6-31G(d) levels of theory, respectively. Figures 4 through 9 show the calculated geometry

TABLE 4: $[(C-H)_{TS} - (C-H)_{Reactant}]/[(O-H)_{TS} - (O-H)_{Product}]$

geometry optimization	$CF_3CCl_2H + OH$	$CF_3CFClH + OH$
HF/6-31G(d)	1.09	1.13
MP2(full)/6-31G(d)	0.46	0.49

at the MP2(full)/6-31G(d) level of theory for CF_3CCl_2H, CF_3CFClH, CF_3CCl_2-H-OH (TS), $CF_3CFCl-H-OH$ (TS), $CF_3C\cdot Cl_2$, and $CF_3C\cdot FCl$, respectively. Bond lengths of C_2-H_8 and H_8-O_9 for CF_3CCl_2-H-OH (TS) and $CF_3CFCl-H-OH$ (TS) were 1.223, 1.261 and 1.228, 1.252 Å, respectively. The bond angles of $\angle C_2H_8O_9$ for CF_3CCl_2-H-OH (TS) and $CF_3CFCl-H-OH$ (TS) were 166.0 and 164.0, respectively. There was no significant difference for the bond lengths of C_1-C_2 between reactants and TSs, but those in products were 0.025 and 0.018 Å shorter than reactants for $CF_3C\cdot Cl_2$ and $CF_3C\cdot FCl$, respectively. The dihedral angles between Cl−Cl and Cl−F at the radical site in reactants were 150.6° and 137.0°, respectively. The parameter $[(C-H)_{TS} - (C-H)_{Reactant}]/[(O-H)_{TS} - (O-H)_{Product}]$ was calculated based on geometries determined by HF/6-31G(d) and MP2(full)/6-31G(d) levels of theory and is shown in Table 4. The calculated parameters were 1.09 and 1.13 for CF_3CCl_2H and $CF_3CCFClH$, respectively, using the HF/6-31G(d) level of theory. The calculated values using the MP2(full)/6-31G(d) level of theory were 0.46 and 0.49 for CF_3CCl_2H and $CF_3CCFClH$, respectively. Calculated O−H bond lengths in H_2O were 0.947 and 0.969 Å with HF/6-31G(d) and MP2(full)/6-31G(d) levels of theory, respectively. The result indicates that TS structures determined by HF/6-31G(d) were in a neutral position between reactant-like and product-like geometry, and those determined by MP2(full)/6-31G(d) exhibited more reactant-like geometry.

Thermodynamic Properties and Hydrogen Bond Dissociation Energy. Table 5 shows calculated thermodynamic properties of reactants. TVR represents the summation of the translational, rotational, and vibrational contributions to $S°_{298}$ and $C_p(T)$. IR represents the hindered internal rotational contribution to $S°_{298}$ and $C_p(T)$.

The rotational barriers for reactants and products were calculated slightly differently. For the reactants, the rotational minimum was calculated at the optimized geometries, and the maximum was calculated by fixing the $F_5C_1-C_2Cl_6$ dihedral angle as eclipsed, yet optimizing elsewhere except for the $F_5C_1-C_2Cl_6$ dihedral angle. The rotational barriers were estimated by taking the relative energy differences between the minimum and maximum, including zpe. Calculated rotational barrier heights using MP2(full)/6-31G(d)-determined energy and HF/6-31G(d)-determined zpe were 6.57 and 5.27 for CF_3CCl_2H and CF_3CFClH, respectively. Values are presented in Table 6. Both molecules were expected to exhibit 3-fold symmetry (periodic with each 120°). For the products, the rotational barriers were estimated by scanning the dihedral angle of $F_5C_1-C_2Cl_6$ by 10° intervals from 0° (optimized configuration) to 180° using the MP2(full)/6-31G(d) level of theory. The geometries were optimized except for the scanned dihedral angle, $F_5C_1-C_2Cl_6$, and the dihedral angle of the two atoms attached to C_2. Both rotational barrier curves exhibit 3-fold symmetry, with barrier heights of 2.79 and 2.96 kcal/mol for $CF_3C\cdot Cl_2$ and $CF_3C\cdot FCl$, respectively. The potential curves were expressed as

$$V(Ø) = 3.28 + 3.28 \times \cos(3Ø) \text{ for } CF_3CCl_2H \quad (10)$$

$$V(Ø) = 2.63 + 2.63 \times \cos(3Ø) \text{ for } CF_3CFClH \quad (11)$$

$$V(Ø) = 1.40 + 1.40 \times \cos(3Ø) \text{ for } CF_3C\cdot Cl_2 \quad (12)$$

$$V(Ø) = 1.48 + 1.48 \times \cos(3Ø) \text{ for } CF_3C\cdot FCl \quad (13)$$

The G2(MP2)-determined energies and experimental values for the isodesmic reactions are presented in Tables 7 and 8, respectively. An experimental enthalpy of formation for ethane was obtained from Pittam et al.[26] 1,1,1-Trifluoroethane and

TABLE 5: Thermodynamic Properties[a]

compound (symmetry #)		$H_f°_{298}$[b]	$S°_{298}$[c]	C_{p300}[c]	C_{p400}	C_{p500}	C_{p600}	C_{p800}	C_{p1000}	C_{p1500}
CF_3CCl_2H(3)	TVR[d]		78.20[g]	22.64	26.64	29.68	31.96	34.97	36.81	39.14
	IR[e]		6.30	2.10	2.19	2.26	2.30	2.20	1.98	1.36
	Total	−178.0	84.50	24.74	28.83	31.94	34.26	37.17	38.79	40.50
	H-BDE[f]	95.3								
CF_3CFClH(3)	TVR		76.00[g]	21.70	25.72	28.87	31.27	34.49	36.47	38.97
	IR		6.41	2.16	2.27	2.33	2.31	2.12	1.85	1.24
	Total	−221.2	83.79[h]	23.86	27.99	31.20	33.58	36.61	38.32	40.21
	H-BDE	99.2								
$CF_3C\cdot Cl_2$(6)	TVR		77.47[g]	22.40	25.73	28.15	29.88	32.04	33.23	34.57
	IR		7.30	2.33	2.22	2.03	1.84	1.50	1.25	0.81
	Total	−134.8	86.15[i]	24.73	27.95	30.18	31.72	33.54	34.48	35.38
$CF_3C\cdot FCl$(3)	TVR		76.30[g]	21.44	24.86	27.41	29.26	31.61	32.93	34.42
	IR		7.07	2.33	2.25	2.09	1.90	1.59	1.35	0.93
	Total	−174.0	84.75[i]	23.77	27.11	29.50	31.16	33.20	34.28	35.35

[a] Thermodynamic properties are referred to a standard state of an ideal gas of pure enantiomeric at 1 atm. Torsional frequencies are excluded in the calculations of entropies and heat capacities. Instead, a more exact contribution from analysis of hindered rotations about C−C is included. See text. [b] Units in kcal/mol. [c] Units in cal/(mol K). [d] Sum of contributions from translations, external rotations, and vibrations. [e] Contribution from internal rotation about C−C bond. [f] Hydrogen bond dissociation energy, unit in kcal/mol. [g] Symmetry number is taken into account (−R × ln(symmetry number)). [h] Contribution for optical isomer (OI) is taken into account (R × Ln(2) = 1.38 cal/(mol K)). [i] Contribution for spin degeneracy is taken into account (R × Ln(2) = 1.38 cal/(mol K)).

TABLE 6: Rotational Barriers for Reactants

	staggered conformation MP2(full)/6-31G(d)[a]	scaled zpe HF/6-31G(d)[a]	scaled torsional frequency[b]	eclipsed conformation MP2(full)/6-31G(d)[a]	scaled zpe HF/6-31G(d)[a]	rotational barrier[c]
CF_3CCl_2H	−1294.661997	0.0339597	71	−1294.65165	0.0339168	6.57
CF_3CHFCl	−934.6459261	0.0356071	72	−934.637683	0.0355910	5.27

[a] Unit in Hartree. [b] The corresponding torsional frequencies were excluded. Unit in cm^{-1}. [c] Unit in kcal/mol.

TABLE 7: G2(MP2) Energies[a]

compound	G2(MP2) energy
CF_3CCl_2H	−1295.382307
CF_3CFClH	−935.394444
CF_3CH_3	−377.116202
CCl_2HCH_3	−997.908773
$CFClHCH_3$	−637.922724
C_2H_6	−79.624450
$CF_3C{\cdot}Cl_2$	−1294.729510
$CF_3C{\cdot}FCl$	−934.735311
C_2H_5	−78.963177
H_2O	−76.326228
OH	−75.637619

[a] Unit in Hartree.

TABLE 8: Experimental Value in use of Isodesmic Reaction[a]

compound	$\Delta H_f°_{298}$	reference
C_2H_6	−20.04 ± 0.07	26
C_2H_5	28.5 ± 0.5	43
CF_3CH_3	−178.94 ± 0.76	27
$CFClHCH_3$	−74.90 ± 0.60	27
CCl_2HCH_3	−30.50 ± 0.26	28

[a] Unit in kcal/mol.

1-chloro,1-fluoroethane were obtained from Kolesov et al.[27] 1,1-Dichloroethane was obtained from Cox et al.[28] These values are recommended in the NIST Standard Reference Database.[42] $\Delta H_f°_{298}$ for CF_3CCl_2H and CF_3CFClH were calculated as −178.0 and −221.2 kcal/mol, respectively. $\Delta H_f°_{298}$ for CF_3CCl_2 and CF_3CFCl were calculated using experimental values of ethane[26] and ethyl radical[43] and calculated values of CF_3CCl_2H and CF_3CFClH. The values were calculated as −134.5 and −174.0 kcal/mol, respectively. Hydrogen BDEs were also estimated using calculated $\Delta H_f°_{298}$ for the reactants and products with experimental values of $\Delta H_f°_{298}$ for the hydrogen atom[29] (52.1 kcal/mol), resulting in values for CF_3CCl_2H and CF_3CFClH of 95.3 and 99.2 kcal/mol, respectively.

Rate Constants. G2(MP2)-determined transition-state energies, forward and reverse energy barriers where zpe were included, adjusted energy barriers, and calculated and adjusted imaginary frequencies are shown in Table 9. Hindered internal rotational contributions for the partition function are calculated and replaced for the corresponding internal rotational partition functions. Rotational barrier heights for C−C rotors for the transition states, CF_3CCl_2−H−OH and CF_3CFCl−H−OH, were assumed to be the same as barrier heights for CF_3CCl_2H and CF_3CFClH, respectively. Those rotational barriers were estimated as 6.57 and 5.27 kcal/mol, respectively. Rotational barriers for CC−OH were estimated by scanning the dihedral angle of $C_1C_2H_8$−O_9H_{10} by 15° intervals from 0° (optimized configuration) to 360° using the HF/6-31G(d) level of theory for both CF_3CCl_2−H−OH and CF_3CFCl−H−OH. Other parameters were fixed while the CCH−OH dihedral was scanned. The rotational barrier heights along CC−OH rotors were 0.95 and 1.28 kcal/mol for CF_3CCl_2−H−OH and CF_3CFCl−H−OH, respectively, and no multiple periodicity was found.

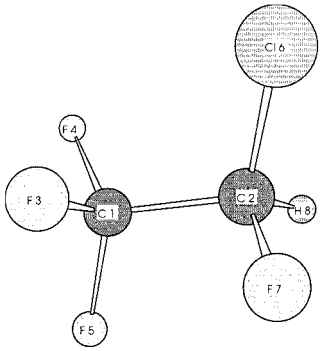

Bond Length	Å	Bond Angle	Degree
C1-C2	1.521	∠C2C1F3	111.7
C1-F3	1.337	∠C2C1F4	110.4
C1-F4	1.343	∠C2C1F5	108.7
C1-F5	1.345	∠C1C2Cl6	111.0
C2-Cl6	1.756	∠C1C2F7	107.1
C2-F7	1.367	∠C1C2H8	109.7
C2-H8	1.090		

Figure 5. MP2(full)/6-31G(d) optimized geometry (CF_3CFClH).

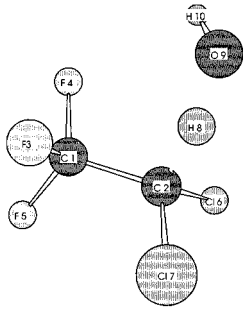

Bond Length	Å	Bond Angle	degree	Dihedral Angle	degree
C1-C2	1.522	∠C2C1F3	110.5	∠C1C2H8O9	-25.9
C1-F3	1.338	∠C2C1F4	109.2	∠C2H8O9H10	-47.3
C1-F4	1.350	∠C2C1F5	112.0		
C1-F5	1.339	∠C1C2Cl6	111.2		
C2-Cl6	1.743	∠C1C2Cl7	111.7		
C2-Cl7	1.739	∠C1C2H8	104.9		
C2-H8	1.223	∠C2H8O9	166.0		
H8-O9	1.261	∠H8O9H10	100.8		
O9-H10	0.980				

Figure 6. MP2(full)/6-31G(d) optimized geometry (CF_3CCl_2−H−OH) (TS).

Both activation energies and imaginary frequencies were adjusted to fit the experimental data for k_1 and k_2. Our first attempt was to adjust the activation energy to fit the experimental data at high temperature, where the tunneling effect is fairly small. The imaginary frequency was then adjusted until an appropriate tunneling correction was obtained to fit the experimental data at low temperature.

Figures 10 and 11 show experimental measurements and model results for k_1 and k_2, respectively. For k_1, the activation energy and the imaginary frequency were adjusted to 2.2 kcal/mol and 2200i, respectively. For k_2, the activation energy and

TABLE 9: Transition State Energies, Energy Barriers, and Imaginary Frequencies[a]

		$\Delta E_e^{\neq}$		ω_i	
reaction	E(G2(MP2)[b]	G2(MP2)[c,d]	adj[e]	HF/6-31G(d)[e]	adj[f]
CF_3CCl_2H + OH	−1371.067394	1.37 (24.25)	2.20 (25.08)	2786i	2200i
CF_3CFClH + OH	−1011.078727	2.65 (21.49)	3.60 (22.44)	2726i	2200i

[a] TS energies in Hartree, energy barriers in kcal/mol, and frequencies in cm^{-1}. [b] G2(MP2) energies at 0 K. Scaled zpe was included. [c] Energy barriers at 0 K. Scaled zpe was included. [d] Quantities in brackets are energy barriers for the reverse reaction. [e] Scaled by 0.8929. [f] See text.

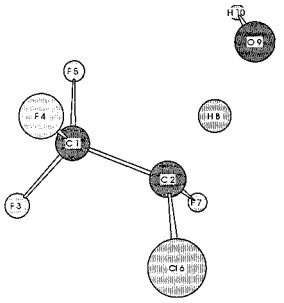

Bond Length	Å	Bond Angle	Degree	Dihedral Angle	Degree
C1-C2	1.519	∠C2C1F3	111.4	∠C1C2H8O9	-2.2
C1-F3	1.339	∠C2C1F4	110.8	∠C2H8O9H10	-59.6
C1-F4	1.337	∠C2C1F5	108.4		
C1-F5	1.348	∠C1C2Cl6	113.4		
C2-Cl6	1.731	∠C1C2F7	108.1		
C2-F7	1.357	∠C1C2H8	106.6		
C2-H8	1.228	∠C2H8O9	164.0		
H8-O9	1.252	∠H8O9H10	100.4		
O9-H10	0.980				

Figure 7. MP2(full)/6-31G(d) optimized geometry ($CF_3CFCl-H-OH$) (TS).

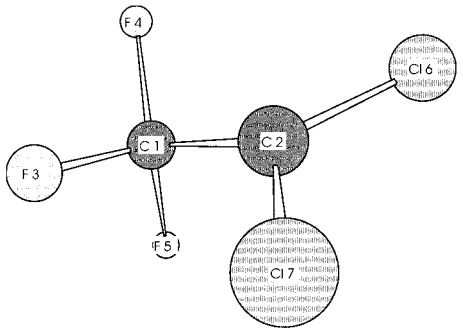

Bond Length	Å	Bond Angle	Degree	Dihedral Angle	Degree
C1-C2	1.500	∠C2C1F3	110.5	∠Cl6C2C1F5	75.3
C1-F3	1.342	∠C2C1F4	110.5	∠Cl7C2C1Cl6	-150.6
C1-F4	1.342	∠C2C1F5	111.7		
C1-F5	1.351	∠C1C2Cl6	117.0		
C2-Cl6	1.695	∠C1C2Cl7	117.0		
C2-Cl7	1.695				

Figure 8. MP2(full)/6-31G(d) optimized geometry (CF_3CCl_2).

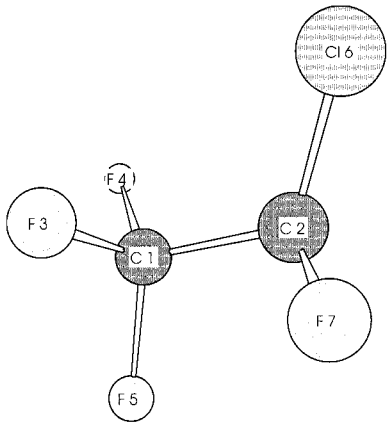

Bond Length	Å	Bond Angle	Degree	Dihedral Angle	Degree
C1-C2	1.503	∠C2C1F3	111.7	∠Cl6C2C1F5	172.8
C1-F3	1.348	∠C2C1F4	110.4	∠F7C2C1Cl6	137.0
C1-F4	1.341	∠C2C1F5	109.4		
C1-F5	1.342	∠C1C2Cl6	117.8		
C2-Cl6	1.698	∠C1C2F7	112.0		
C2-F7	1.337				

Figure 9. MP2(full)/6-31G(d) optimized geometry (CF_3CFCl).

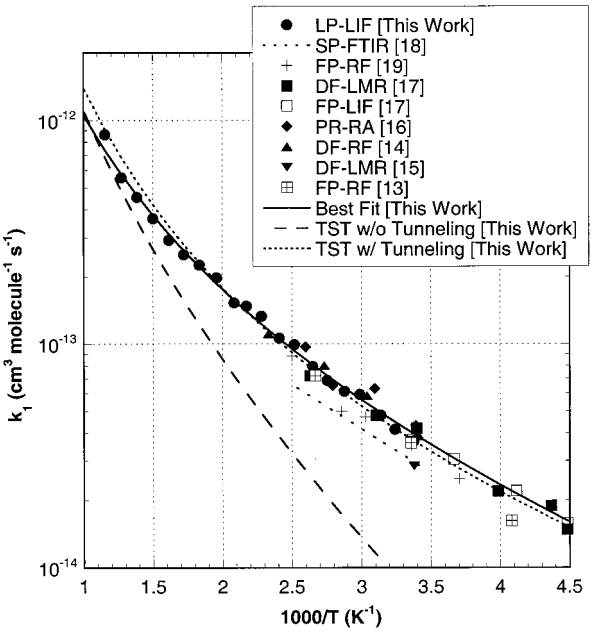

Figure 10. Arrhenius plot of experimental measurements for k_1. Also shown are ab initio-based bimolecular TST curves with and without an Eckart tunneling correction and the empirical "best fit" curve through the data.

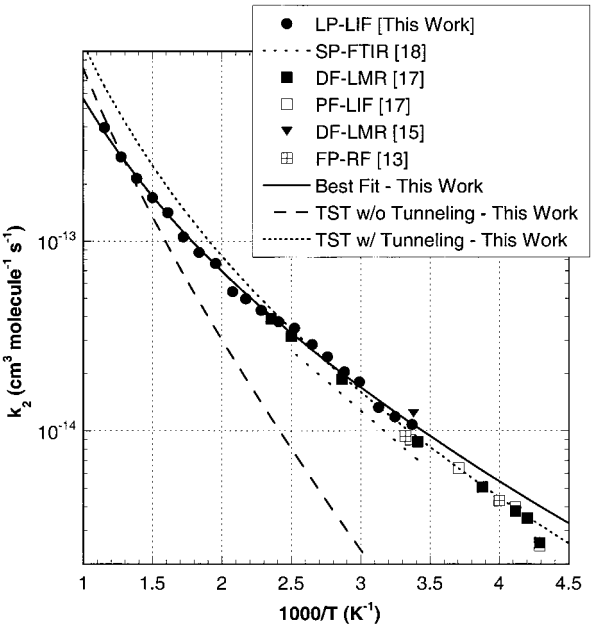

Figure 11. Arrhenius plot of experimental measurements for k_2. Also shown are ab initio-based bimolecular TST curves with and without an Eckart tunneling correction and the empirical "best fit" curve through the data.

the imaginary frequency were also adjusted to 3.6 kcal/mol and 2200i, respectively. Table 10 presents the calculated temperature dependence and tunneling factor, and Table 11 presents calculated and experimental three-parameter fits for k_1 and k_2, respectively.

Comparison of Model Predictions. Comparisons of our bimolecular TST model with previous TST[8] and SAR[9] calculations are also shown in Table 11. For k_1, the previous TST model is in good agreement with our calculation at room temperature but underestimates the rate coefficient by a factor of 2 at 1000 K. The SAR calculation is a factor of 3 lower than our TST model results below 400 K. The deviation decreases to below 50% between 500 and 1000 K. Our TST model for k_1 shows

TABLE 10: Temperature Dependence of Calculated Rate Constants and Tunneling Corrections[a]

	$CF_3CCl_2H + OH$		$CF_3CFClH + OH$	
T(K)	k_1	Γ	k_2	Γ
250	2.18E−14	6.13	4.52E−15	17.9
298	3.75E−14	4.08	9.81E−15	9.22
400	9.13E−14	2.47	3.32E−14	4.10
500	1.79E−13	1.89	8.13E−14	2.69
600	3.08E−13	1.60	1.65E−13	2.08
800	7.03E−13	1.33	4.94E−13	1.58
1000	1.42E−12	1.21	1.12E−12	1.37
1500	4.63E−12	1.09	4.52E−12	1.17
2000	1.04E−11	1.05	1.13E−11	1.10

[a] Rate constants in units of cm^3 $molecule^{-1}$ s^{-1}.

TABLE 11: Calculated and Experimental "Arrhenius" Fit Parameters for $k = AT^n e^{-B/T}$

reaction		A^a	n	B^b	range[b]
$CF_3CCl_2H + OH$	calc.	3.25E−21	2.88	52	250−2000
	expt.	2.20E−19	2.26	226	296−866
	SAR[9]	1.89E−18	2.0	636	250−1250
	TST[8]	7.30E−18	1.7	370	250−2000
$CF_3CFClH + OH$	calc.	4.52E−22	3.18	362	250−2000
	expt.	7.72E−20	2.35	458	297−867
	SAR[9]	1.89E−18	2.0	1037	250−1250
	TST[8]	1.23E−17	1.7	720	250−2000

[a] Units in cm^3 $molecule^{-1}$ s^{-1}. [b] Units in Kelvin.

good agreement with our experimental data as well as other experimental results through the entire temperature range. For k_2, the previous TST model predicts rate constants about 80% larger than our calculation at 250 K. The deviation decreases to about 50% at 1000 K. The SAR calculation is a factor of 3 below our calculation at 250 K. The deviation decreases to about 60% at 1000 K. Our TST model for k_2 shows good agreement with both our experimental results and others at temperatures below 500 K but overestimates the experimental data at 800 K by ∼60%. The model shows stronger temperature-dependent curvature than demonstrated by our experimental measurements.

Summary

New rate measurements for the gas-phase reaction of OH radicals with CF_3CCl_2H and CF_3CFClH are reported. The measurements, obtained over a wide temperature range, exhibited curvature and were best described by modified Arrhenius expressions. Ab initio-based transition state-theory calculations, with the incorporation of an asymmetrical Eckart tunneling correction, provided reasonable fits to these data and prior data sets. Thermochemical data for these two reactions were also provided as a result of the ab initio calculations. The results of this study indicate that F substitution at the reaction site has a significant (reductive) effect on HCFC reactivity. This result was also observed in our prior studies of $CHFCl_2$ and CHF_2Cl.[4] A similar effect in HCFC reactivity was not observed for changes in F substitution β to the reaction site, indicating the electron-withdrawing effects of the F atoms are limited to the vicinity of the reaction site.

Acknowledgment. T.Y., T.F, and P.T. acknowledge support from the Environmental Protection Agency (Grant R819861-01-0). R.B. acknowledges the Air Force Office of Scientific Research and the Materials Directorate at Wright Laboratory for financial support and computational resources. The authors thank Dr. Paul Marshall for his generous help and advice for the theoretical calculations.

References and Notes

(1) Atkinson, R. *J. Phys. Chem. Ref. Data* 1989, Monograph 1.
(2) Tsang, W. *Combust. Sci. Technol.* **1990**, *74*, 99.
(3) Senkan, S. M. Survey of Rate Constants in the C/H/Cl/O System. In *Combustion Chemistry*, 2nd ed.; Gardiner, W. C., Jr., Ed.; in press.
(4) Fang, T. D.; Taylor, P. H.; Dellinger, B. *J. Phys. Chem.* **1996**, *100*, 4048.
(5) Fang, T. D.; Taylor, P. H.; Dellinger, B.; Ehlers, C. J.; Berry, R. J. *J. Phys. Chem. A* **1997**, *101*, 5758.
(6) Fang, T. D.; Taylor, P. H.; Berry, R. J. *J. Phys. Chem. A* **1999**, *103*, 2700.
(7) Cohen, N.; Benson, S. W. *J. Phys. Chem.* **1987**, *91*, 162.
(8) Cohen, N.; Westberg, K. R. *J. Phys. Chem. Ref. Data* **1991**, *20*, 1211.
(9) Atkinson, R. *Int. J. Chem. Kinet.* **1986**, *18*, 555.
(10) Estimated using G2(MP2) theory. See Table 7.
(11) Fang, T. D. Ph.D. Dissertation, University of Dayton, 1996.
(12) DeMore, W. B.; Sander, S. P.; Golden, D. M.; Hampson, R. F.; Kurylo, M. J.; Howard, C. J.; Ravishankara, A. R.; Kolb, C. E.; Molina, M. J. *Chemical Kinetics and Photochemical Data for Use in Stratospheric Modeling;* Evaluation No. 12; Jet Propulsion Laboratory: 1997.
(13) Simonaitis, R.; Heicklen, J. *J. Phys. Chem.* **1973**, *77*, 1932.
(14) Watson, R. T.; Machado, G.; Conaway, S.; Wagner, S.; Davis, D. D. *J. Phys. Chem.* **1976**, *81*, 256.
(15) Clyne, M. A. A.; Holt, P. M. *J. Chem. Soc., Faraday Trans. 2* **1979**, *75*, 582.
(16) Howard, C. J.; Evenson, K. M. *J. Chem. Phys.* **1976**, *64*, 1618.
(17) Nielsen, O. J.; Pagsberg, P.; Sillesen, A. *Third European Symposium on the Physico-Chemical Behavior of Atmospheric Pollutants*; Riedel: Boston, 1984; p 283.
(18) Gierczak, T.; Talukdar, R.; Vaghjiani, G. L.; Lovejoy, E. R.; Ravishankara, A. R. *J. Geophys. Res.* **1991**, *96*, 5001.
(19) Hsu, K.-J.; DeMore, W. B. *J. Phys. Chem.* **1995**, *99*, 1235.
(20) Lui, R.; Huie, R. E.; Kurylo, M. J. *J. Phys. Chem.* **1990**, *94*, 3247.
(21) Frisch, M. J.; Trucks, G. W.; Schlegel, H. B.; Gill, P. M. W.; Johnson, B. G.; Robb, M. A.; Cheeseman, R. J.; Keith, T.; Petersson, G. A.; Montgomery, J. A.; Raghavachari, K.; Al-Laham, M. A.; Zakrzewski, V. G.; Ortiz, J. V.; Foresman, J. B.; Cioslowski, J.; Stefanov, B. B.; Nanayakkara, A.; Challacombe, M.; Peng, C. Y.; Ayala, P. Y.; Chen, W.; Wong, M. W.; Andres, J. L.; Replogle, E. S.; Gomperts, R.; Martin, R. L.; Fox, D. J.; Binkley, J. S.; Defrees, D. J.; Baker, J.; Stewart, J. P.; Head-Gordon, M.; Gonzalez, C.; Pople, J. A. Gaussian 94; Gaussian, Inc.: Pittsburgh, PA, 1995.
(22) Frisch, M. J.; Trucks, G. W.; Schlegel, H. B.; Scuseria, G. E.; Robb, M. A.; Cheeseman, J. R.; Zakrzewski, V. G.; Montgomery, J. A.; Stratmann, R. E.; Burant, J. C.; Dapprich, J. M.; Millan, J. M.; Daniels, A. D.; Kudin, K. N.; Strain, M. C.; Farcas, O.; Tomasi, J.; Barone, v.; Cossi, M.; Cammi, R.; Mennucci, B.; Pomelli, c.; Adamo, C.; Clifford, S.; OChterski, J.; Petersson, G. A.; Ayala, P. Y.; Cui, Q.; Morokuma, K.; Marick, D. K.; Rabuck, A. D.; Raghavachari, K.; Foresman, J. B.; Cioslowski, J.; Ortiz, J. V.; Stefanov, B. B.; Liu, G.; Liashenko, A.; Piskorz, P.; Komaromi, I.; Gomperts, R.; Martin, R. L.; Fox, D. J.; Keith, T.; Al-Laham, M. A.; Peng, C. Y.; Nanayakkara, A.; Gonzalez, C.; Challacombe, M.; Gill, P. M. W.; Johnson, B.; Chen, W.; Replogle, E. S.; Pople, J. A. Gaussian98; Gaussian, Inc.: Pittsburgh, 1998.
(23) Curtiss, L. A.; Raghavachari, K.; Pople, J. A. *J. Chem. Phys.* **1993**, *98*, 1293.
(24) Hehre, W. J.; Radom, L.; Schleyer, P. R.; Pople, J. A. *Ab Initio Molecular Orbital Theory*; John Wiley & Sons: New York, 1986; Chapter 6.
(25) Lay, T. H.; Krasnoperov, L. N.; Venanzi, C. A.; Bozzelli, J. W. *J. Phys. Chem.* **1996**, *100*, 8240.
(26) Pittam, D. A.; Pilcher, G. *J. Chem. Soc., Faraday Trans. 1* **1972**, *68*, 2224.
(27) Kolesov, V. P.; Papina, T. S. *Russ. Chem. Rev.* **1983**, *52*, 425.
(28) Cox, J. D.; Pilcher, G. *Thermochemistry of Organic and Organometallic Compounds*; Academic Press: New York, 1970.
(29) Lide, D. R. *CRC Handbook of Chemistry and Physics*, 80th ed.; CRC Press: Boca Raton, FL, 1988−1989; p 5−17.
(30) Krasnoperov, L. N.; Lay, T. H.; Shokhirev, N. V. *Thermodynamic Properties of Hindered Rotor by Diagonalization of Hamiltonian Matrix* (in preparation). The computer code "ROTATOR" is available: http://www.chem.arizona.edu/faculty/walk/nikolai/programs.html.
(31) Yamada, T.; Lay, T. H.; Bozzelli, J. W. *J. Phys. Chem.* **1998**, *102*, 7286.
(32) McQuarrie, D. A. *Statistical Mechanics*; Harper & Row: New York, 1976.
(33) Yamada, T.; Bozzelli, J. W. *J. Phys. Chem.* **1999**, *103*, 5602.
(34) Chen, S.S.; Rodgers, A. S.; Chao, R. C.; Wilhoit, R. C.; Zwolinski, B. J. *J. Phys. Chem. Ref. Data* **1975**, *4*, 441.
(35) Eyring, H. J. *J. Chem. Phys.* **1935**, *35*, 107.

(36) Hill, T. L. *An Introduction to Statistical Thermodynamics*; Addison-Wesley Publishing Co.: Reading, MA, 1960.
(37) Schwartz, M.; Marshall, P.; Berry, R. J.; Ehlers, C. J.; Petersson, G. A. *J. Phys. Chem.* **1998**, *102*, 10074.
(38) Chase, Jr. *NIST-JANAF Thermochemical Tables*, 4th ed.; *J. Phys. Chem. Ref. Data*, **1998**, Monograph 9, 1−1951.
(39) Ayala, P. Y.; Schlegel, H. B. *J. Chem. Phys.* **1998**, *108*, 2314.
(40) Eckart, C. *Phys. Rev.* **1930**, *35*, 1203.
(41) Petersson, G. A.; Schwartz, M. Personal communication.
(42) NIST Chemistry Webbook. Linstrom, P. J., Mallard, W. G., Eds.; http://webbook.nist.gov/chemistry/(1998).
(43) Tsang, W. *Heats of Formation of Organic Free Radicals by Kinetic Methods in Energetics of Organic Free Radicals*; Blackie Academic and Professional: London, 1996; pp 22−58.